

2006

Progress on a Photovoltaic Cell Design Consisting of Silicon Nanowires and Poly (3- hexylthiophene)

Lori Noice
Portland State University

Follow this and additional works at: <https://pdxscholar.library.pdx.edu/mcnair>

Let us know how access to this document benefits you.

Recommended Citation

Noice, Lori (2006) "Progress on a Photovoltaic Cell Design Consisting of Silicon Nanowires and Poly (3-hexylthiophene)," *PSU McNair Scholars Online Journal*: Vol. 2: Iss. 1, Article 28.
<https://doi.org/10.15760/mcnair.2006.309>

This open access Article is distributed under the terms of the [Creative Commons Attribution-NonCommercial-ShareAlike 4.0 International License \(CC BY-NC-SA 4.0\)](#). All documents in PDXScholar should meet [accessibility standards](#). If we can make this document more accessible to you, [contact our team](#).

**Progress on a photovoltaic cell design consisting of silicon nanowires and poly
(3- hexylthiophene)**

by
Lori Noice

Faculty Mentor:
Rajendra Solanki

Citation: Noice, Lori. Progress on a photovoltaic cell design consisting of silicon nanowires and poly (3- hexylthiophene). Portland State University McNair Scholars Online Journal, Vol. 2, 2006-2008: pages [309-319].

Progress on a photovoltaic cell design consisting of silicon nanowires and poly(3-hexylthiophene)

Lori Noice¹, Gary Goncher¹, Raj Solanki^{1,2}

¹ Department of Physics, Portland State University, P.O. Box 751, Portland, OR 97206-0751

² Department of Computer Science and Electrical Engineering, Oregon Graduate Institute, Beaverton, OR 97006-8921

Abstract

A bulk-heterojunction photovoltaic cell design made from silicon nanowires (SiNW) and poly(3-hexylthiophene) (P3HT) could provide the photon absorption and charge transport needed for a high efficiency hybrid PV cell. Since the mechanisms associated with the inorganic/organic semiconductor heterojunction are not yet well understood, the simple design of the proposed PV cell and tunable properties of both SiNW and P3HT affords experimental optimization opportunities.

Introduction

For decades, solar radiation has been a strong candidate for an ecologically friendly and globally sustainable energy source. Indeed, covering only 0.16 % of the Earth's surface with commercially available 10 % efficiency PV cells would provide almost double the world's collective energy needs [1]. Yet, despite a steady increase in PV power system installations (~36 % a year from 2000-2004¹), PV power remains unfamiliar to utilities companies and the general public alike due to high production costs [2]. At around \$3 Watt/hour to produce, PV power is a cost effective energy solution for only the most remote locations², and in order for PV power to become competitive with other renewable energy markets (e.g. hydroelectric or wind generated electricity), the production costs must be reduced by an order of magnitude [2,3].

The majority of the commercially available PV power systems are made from single crystalline silicon or amorphous silicon (c-Si and a-Si, respectively), with power conversion efficiencies (PCE) between 11 - 25 % [2]. About half of the total production cost involved with these systems is associated with the Si purification and production, which involves temperatures in excess of 1400 °C, vacuum systems, clean rooms, chlorinated compounds, and large amounts of water, energy, and feedstock waste [4,5]. Thin film PV cells utilizing CdTe (cadmium telluride) or CdSe offer similar efficiencies [2,6], however there are environmental

concerns with production and disposal of PV cells containing heavy metals. The weight, appearance, and brittleness of inorganic PV cells have also contribute to the lack of PV power implementation through high shipping costs and limited architectural integration capabilities [3].

In response to the shortcomings of inorganic PV cells and aided by advancements in organic photoelectric materials for photodetectors, FETs, and LEDs, organic PV cells have become the object of intensive research in recent years. Organic thin film PV cells made from semiconducting polymers are light weight [7], low in toxicity, offer dramatic reductions in processing costs [3,8,9-12], tunable optical properties [7,13,14], as well as mechanical flexibility and durability [15]. However, the PCEs of organic PV cells are typically less than 2 % and no greater than 5 % [7,10-13,16-19]. The efficiencies of these PV cells are limited by the intrinsically low carrier concentrations and mobilities of polymers [15,19,20]. Many photoactive layer architectures have been devised to overcome these limitations by creating high surface area heterojunctions and alternate charge transport routes through the incorporation of nanostructures, including polymer/fullerene [9,10,15,21], polymer/metal oxide [21-24], and polymer/traditional semiconductor heterojunctions [3,10,21,24,25]. Most of these architectures rely on percolation pathways which present their own efficiency issues, namely, the presence of structural traps resulting in charge build up and the recombination of photogenerated charge carriers [10,21,24,26,27].

This paper reports on the progress of a hybrid inorganic/organic PV cell design which has the potential of providing affordable solar energy. The photoactive layer of the proposed PV cell would be a bulk heterojunction constructed of silicon nanowires (SiNWs) and poly(3-hexylthiophene) (P3HT). SiNWs could potentially be considerably cheaper to produce than either c-Si or a-Si while retaining the capacity for high degrees of crystallinity and purity. P3HT has been shown to absorb more of the optical spectrum than other polymer semiconductors [2,19,28-30,32,33] and has the highest reported mobility [15,29,31]. P3HT also offers the advantage of a variety of wet processing methods which are

¹ Out of the twenty participating countries, 88 % of the installations were in Germany, Japan, and the United States [2]

² e.g. Kenya has one of the few spontaneous PV power markets existing without government subsidies [2]

easily upgradeable to large scale production [19]. Both of these materials possess tunable optical and electronic properties and, working together, could potentially overcome some of the inadequacies and setbacks found in previous hybrid PV cell designs.

SiNW/P3HT PV cell design

Figure 1 shows the proposed architecture for the SiNW/P3HT PV cell. The SiNWs would be anchored to a substrate of c-Si with the n-type P3HT completely surrounding and slightly covering them to create an extended heterojunction throughout the photoactive layer and unbroken pathways to the electrodes of the cell. Like most semiconducting polymers, P3HT is p-type [19,24], therefore, the SiNWs would be doped n-type. The cathode would be a fine Au mesh placed on top of the P3HT, and the anode: a thin Al film deposited on the underside of the c-Si substrate. Figure 2 is the energy band diagram of the constituent materials of the SiNW/P3HT PV cell.

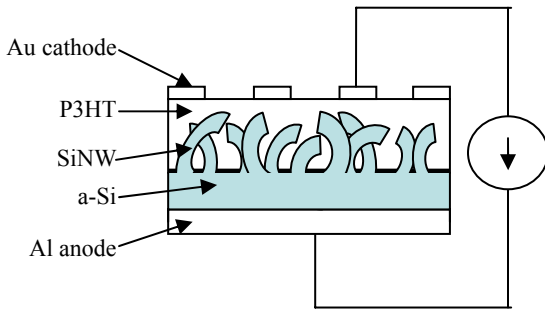


Figure 1: The Proposed SiNW/P3HT PV cell. The P3HT would completely coat the SiNWs creating an extended p-n junction throughout the photoactive layer. The cathode would be a Au grid and the anode would be an Al thin film. The nanowires would be anchored onto a more heavily doped substrate of n-type c-Si.

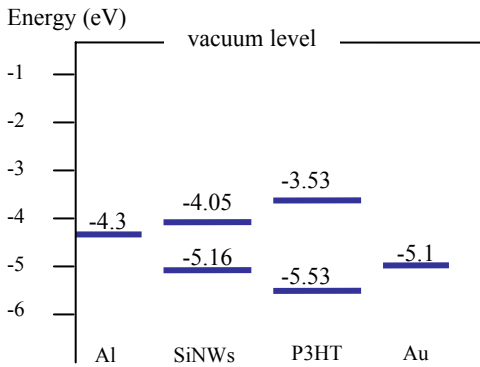


Figure 2: The energy band diagram showing the HOMO and LUMO levels of the P3HT [18,19,28,30,32,33], the band gap of the Si [34], and the work functions of the two electrodes [35].

For this PV cell, both the SiNWs and the P3HT would act as absorbers and carrier transporters [36].

Power conversion efficiency

The PCE (η_{power}) of a PV cell is defined as the power produced by the PV cell divided by the radiant power incident on the cell. The power produced by the PV cell (P_{out}) is equal to the current at the maximum power point (I_{MP}) times the voltage at maximum power point (V_{MP}). This value corresponds to the short circuit current (I_{SC}) times the open circuit (V_{OC}) times a quality factor called the fill factor (FF) [19].

$$\eta_{power} = \frac{P_{out}}{P_{in}} = \frac{I_{MP} \cdot V_{MP}}{P_{in}} = \frac{I_{SC} \cdot V_{OC} \cdot FF}{P_{in}} \quad (4)$$

The relationship between these variables can be seen in the I-V curve of a PV cell. Figure 3 is a generic I-V curve of a hypothetical PV cell. The dashed line represents the functioning of the cell in the dark, where virtually no current would flow in the circuit until a forward bias greater than the open circuit voltage is applied and the contacts would begin to inject charge into the circuit. The dark line represents the cell functioning under illumination (current flows in the opposite direction than when in the dark). The maximum photogenerated current would be under short circuit conditions, and the maximum potential of the cell would be at open circuit [19,37].

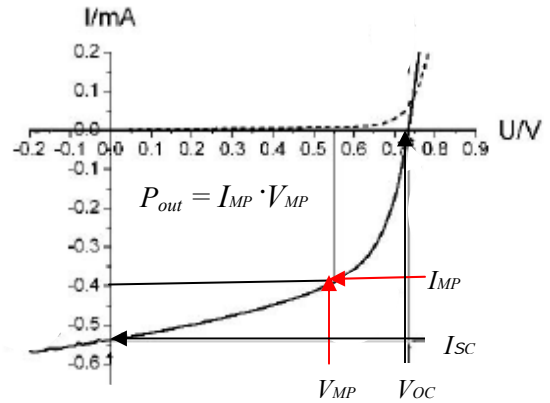


Figure 3: A hypothetical I-V curve for a generic PV cell. The values of V_{MP} and I_{MP} are defined by the largest area rectangle that may fit under the I-V curve. The FF is the fraction of this area to the area contained within the values I_{SC} and V_{OC} . (Adapted from [19])

Ideally, the power generated by the cell would be $P_{ideal} = I_{SC} \cdot V_{OC}$, however, the actual operating power of the cell (P_{out}) is defined by the largest area

rectangle that may be placed under the I-V curve. This rectangle identifies the maximum power operational parameters of the cell V_{MP} and I_{MP} , and its area is equal to $P_{out} = I_{MP} \cdot V_{MP}$. The FF would be the fraction of P_{out} to P_{ideal} , and has a value between 0 and 1 [19,37].

$$FF = \frac{P_{out}}{P_{ideal}} = \frac{I_{MP} \cdot V_{MP}}{I_{SC} \cdot V_{OC}} \quad (1)$$

Modeling a PV cell

A PV cell may be modeled as a current source in parallel with a junction [16,19,31,37]. Figure 4a.) shows an idealized PV cell, where the current in the circuit (I) would be:

$$I = I_s e^{\left(\frac{eV_{out}}{kT} - 1\right)} - I_{ph} \quad (2)$$

The first term represents the dark current, where I_s is the saturation current under reverse bias, e is the electron charge, V_{out} is the voltage across the external load, k is the Boltzmann constant, T is the temperature in K, and I_{ph} is the illumination dependent current.

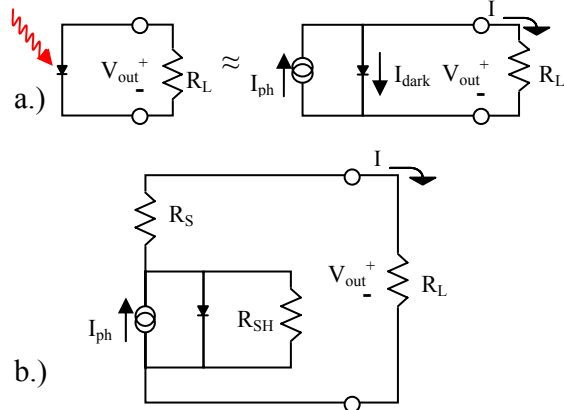


Figure 4: The equivalent circuit of a PV cell. a.) The incident photon induces a current I_{ph} , which may be modeled as a current source in parallel with a junction, where R_L is the load of the external circuit. b.) The schematic is modified to account for losses in the circuit due to the resistance of constituent materials (R_S) and recombination losses as well as structural defects (R_{SH}).

In a real PV cell, non-radiative losses must be accounted for by the presence of series and shunt resistances (R_S and R_{SH} , respectively). Contributions to R_S include the resistances at material interfaces and the resistivity of the constituent materials; R_{SH} accounts for leaks and shorts in the circuit [31,37].

Figure 4b.) depicts the equivalent circuit of a PV cell as an imperfect current source, where the current in the circuit may be modeled as:

$$I = I_s e^{\frac{eV}{nkT}(V_{out} - IR_S)} - 1 \quad (3)$$

An ideality factor n , with a value between 1 and 2, has been introduced for the junction³ [16,37]. This may be rewritten as:

$$I = I_s \left(1 + \frac{R_S}{R_{SH}}\right) - \frac{V_{out}}{R_{SH}} + I_{ph} \quad (4)$$

The shape of the PV cell's I-V curve is heavily dependent on the values of R_S and R_{SH} . Increases in R_S would result in a decreased I_{SC} .

The V_{OC} of the PV cell is dictated by the band gaps of the semiconductors and the difference between the work functions of the electrodes [19]. The relationship between V_{OC} and I_{SC} is derived assuming ideal conditions (i.e. $R_{SH} = \infty$ and $R_S = 0$; $I_{ph} = I_{SC}$ and $I = 0$):

$$V_{OC} = \frac{nkT}{e} \ln \left(\frac{I_{SC}}{I_s} + 1 \right) \quad (5)$$

For a high V_{OC} , the R_{SH} should be as high as possible.

Inorganic and organic semiconductors

The efficiency of an inorganic/organic hybrid solar cell would be affected by the intrinsic differences in the ways the two types of semiconductors photogenerate and transport charges.

A highly crystalline lattice of Si creates a well formed band energy structure which permeates the entire material. Incident photons absorbed by the Si lattice immediately generate charge carriers in the valence and conduction bands (E_V and E_C , respectively). The photogenerated charge carriers are then pulled away from one another by the internal electric fields set up within the PV cell by the p-n junction and judicious choices of contacts [34]. Figure 5 is a schematic of a band structure material exhibiting the photoelectric effect. For inorganic semiconductors like Si, the energy difference between E_V and E_C (the band gap) is equal to both the optical energy gap (E_{OG}), which is the amount of energy that a photon must impart to the Si lattice to

³ This factor accounts for tunneling and recombinations within the diode. A value of 1 represents a perfect diode, and 2 would indicate recombination processes are dominant [31].

excite charge carriers, and to the electrical energy gap (E_{EG}), which is the energy difference between the charge carriers.

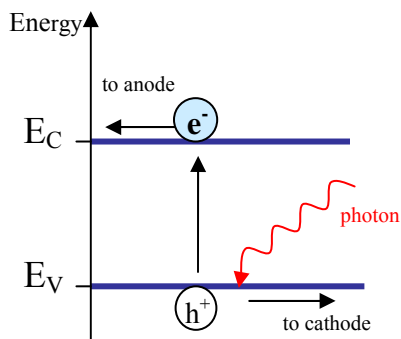


Figure 5: The photoelectric effect in a semiconductor material such as Si. An incident photon excites an electron (e^-) from the valence band (E_V) to the conduction band (E_C), leaving behind a hole (h^+) in the E_V . Internal electric fields within the PV cell would then draw the two charged carriers away from one another towards their respective electrodes.

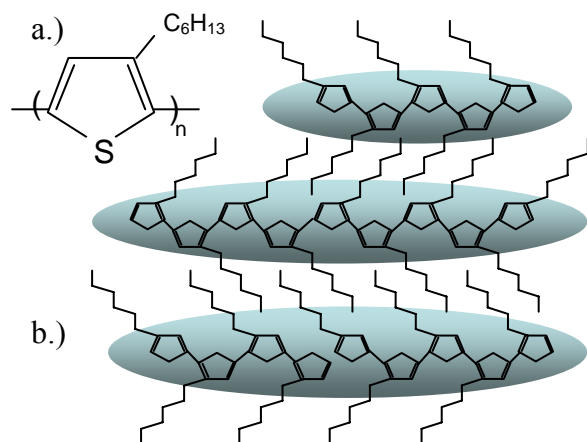


Figure 6a.) The poly(3-hexylthiophene) polymer unit. b.) A portion of the regioregular P3HT polymeric lattice (actual molecules would be over 150 units long) showing band-like energy states extending along the backbone of the thiophene chain. These band-like states are localized to individual molecular units [38,39].

These band-like energy states are associated with the π - bond, or the highest occupied molecular orbital (HOMO), and the π^* - bond, or the lowest occupied molecular orbital (LUMO) [38,39]. These states roughly correlate to the E_V and the E_C of an inorganic semiconductor, respectively [38], and dominate both the optical absorption and charge transport properties of the material [17].

Polymers do not form extended well-ordered crystal lattices due to their molecular size and the arrangements of their constituent atoms. Therefore, well-formed band energy states which permeate the entire material do not occur. Conjugated π - bonds, like those forming the thiophene backbone of P3HT, however, have a wide enough spatial energy distribution between the bonding and anti-bonding states (π and π^* , respectively) to form localized band-like energy states in polymers (i.e. in molecules consisting of ~ 50 or more units) [37]. Figure 6 shows the P3HT molecular unit and illuminates the localized nature of the band-like π - π^* bonds along the thiophene backbones within a P3HT lattice.

The energy difference between the HOMO and LUMO states may be regarded as the band gap of an inorganic semiconductor, yet a thin polymer film cannot be fully described by the band model [31,40]. While, like an inorganic semiconductors, the energy gap between the HOMO and LUMO states is equal to the E_{OG} , it is not equal to the E_{EG} between charge carriers. This is due to the fact that charge carriers are not generated upon absorption of a photon by the polymer lattice. Instead, an excited but electrically neutral state, called an exciton⁴, is created which requires additional energy (E_B) to separate into charge carriers [38,41]. This energy is gained from the offset of energy states at the heterojunction [41-46].

$$E_{EG} = E_{OG} + E_B \quad (6)$$

Figure 7 gives a band diagram for the p-n junction formed in an inorganic/organic PV cell. The exciton is formed by the absorption of a photon by the organic p-type polymer, and then diffuses to the heterojunction where it dissociates into charge carriers by the electric field created by the p-n junction. The h moves back into the HOMO state of the p-type polymer while the e is transferred to the E_C of the n-type inorganic semiconductor [17,38,41]. Therefore, there are two different transport mechanisms taking place simultaneously within the polymer semiconductor: the transport of electrically neutral excitons to the p-n junction, and the transport of the charge carrier to the electrode.

⁴ Since the dielectric constant of polymers is low, and the electronic interaction between the molecules are weak (non-covalent bonding), the Coulombic potential well around the e^- and h^+ conjugate pair is extended, while the carrier's wave functions are restricted. This allows each carrier's wave function to be inside the potential well of the other [41,48,49].

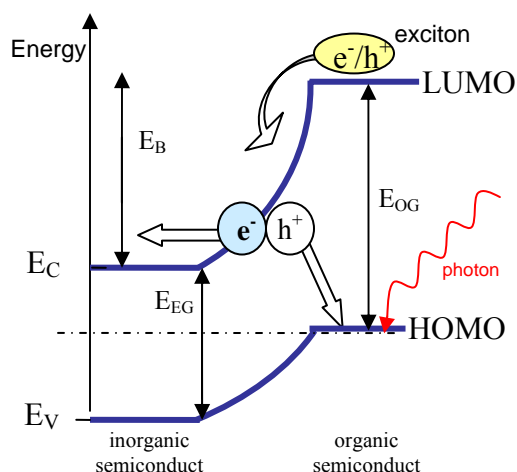


Figure 7: The band offset diagram for the p-n junction of a hybrid PV cell. The values of E_{OG} , E_B , and E_{EG} are those of the organic p-type polymer. An exciton is formed upon absorption of a photon in the organic semiconductor and diffuses to the heterojunction. There it is dissociated into charge carriers by the energy band offset of the p-n junction. The e^- is transferred to the E_C of the n-type inorganic semiconductor and the h^+ moves back into the HOMO state of the organic polymer [38,41]. Optimally, the photon would be absorbed within the depletion region of the p-n junction where the exciton would be immediately split into charge carriers.

Since the LUMO states of adjacent molecular units do not merge completely to form a continuous energy band, the exciton that is formed upon the absorption of a photon into an organic semiconductor lattice is confined to the localized LUMO state of the absorbing molecule (see Figure 6b). The electrically neutral [31,48] exciton propagates through the semiconductor by hopping from one LUMO state to the next via thermal energy transfer [17]. This diffusion, therefore, is random and may be in any direction [38]. At the same time, the exciton is in the process of decaying back to its ground state, either radiatively or non-radiatively. This decay is on a time scale of pico- or nano- seconds, giving diffusion lengths ranging from 1-10 nm [19,17,36]. Excitons may also get trapped by impurities or defect sites, which either contribute to exciton loss or dissociate the exciton into a trapped carrier and a free carrier. The latter, however, is not generally productive towards photogenerated current [31,41].

The E_B s of organic semiconductors are predominately Coulombic and range from 0.05 eV to 1.0 eV [24,31,38,41,43]. Once at the p-n junction, the energy band offset between the organic semiconductor's LUMO state and the inorganic semiconductor's E_C must be greater than the E_B of the exciton [41].

Immediately upon charge carrier generation, the carriers may recombine via the potential drop between the E_C of the inorganic phase and the HOMO state of the organic phase or by Coulombic forces [38]. Although the forces driving recombination are partially those driving charge separation (i.e. band off-set energies and kinetic factors [31,41]), the rate of charge recombination are many orders of magnitude slower than the rate of charge separation [38,42].

Once the charge carriers have been generated at the p-n junction, the hole works its way back through the organic semiconductor to the cathode via both intra- and inter-band transport [14]. Figure 8 depicts how the charge carrier either drifts along one of the localized band-like state under the influence of the PV cells internal electric potential or “hops” to a neighboring band like state. The oxidation/reduction reaction of the inter-band transport may be described by the multiple trap and release model (MTR) (sometimes used to describe charge transport in a-Si) [37].

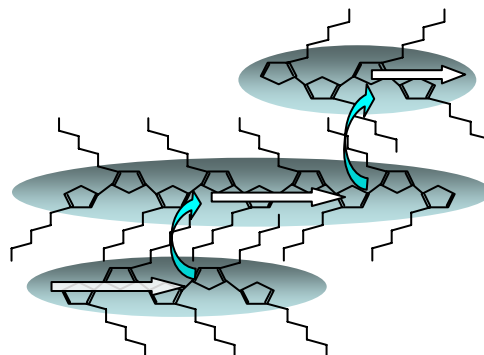


Figure 8: The two different types of charge carrier transport within the polymeric lattice of the organic semiconductor. The white arrows represent the intra-band transport which is propelled by the internal electric potentials of the PV cell, and the blue arrows show the inter-band transport, which may be modeled by MTR.

In the MTR model, the charge carrier forms a polaron with the localized band-like state by coupling with either phonons or lattice deformations induced by the presence of the carrier. The polarons are treated as defect states between the HOMO and LUMO bands; thus, the carriers move through the polymeric lattice by becoming repeatedly trapped/self-trapped by and then thermally released from the localized band-like states. This type of inter-band transport is only field dependent under relatively large electric fields⁵. Figure 9 illuminates

⁵ Electric fields on the order of 10^5 V/cm² are sufficient to modify the Coulombic potentials near trapping levels enough to increase

the processes of photogenerated current in an organic semiconductor, from photon absorption to electricity, with the undesired heat-generating processes appearing in the third column.

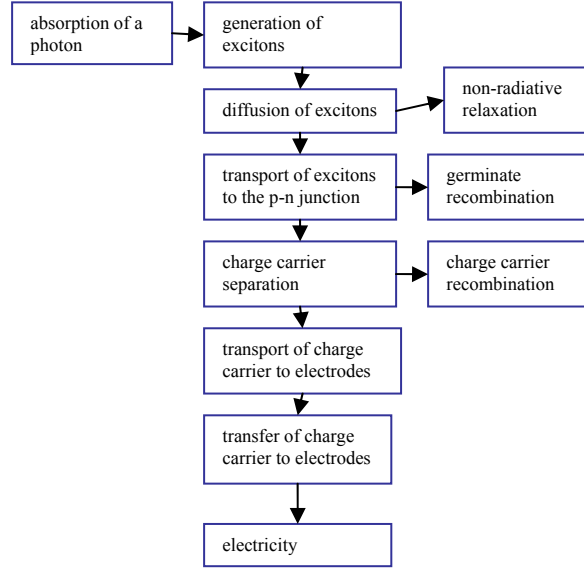


Figure 9: The many stages of photogenerating current in organic semiconductors, with the potentially heat-generating losses in the third column. The additional steps, as compared to inorganic semiconductors, contribute to the lower efficiencies of organic PV cells. The adapted from [14].

PCE of the SiNW/P3HT PV cell

The PCE (η_{power}) of a hybrid PV cell is the sum of the PCEs of the constituent materials, where not only are the materials acting in tandem, but there functional properties are also dependent on one another so that many of these terms are interdependent.

$$\eta_{power} = \eta_{in} + \eta_{org} \quad (7)$$

Many of the physical processes involved with the functioning of a hybrid PV cell are not yet fully understood, yet, once individually addressed, the efficiencies of each component of the cell may be experimentally optimized.

The PCE of SiNWs involves the efficiencies of photon absorption (η_{in-abs}) and charge carrier transport to the electrodes of the PV cell ($\eta_{in-trans}$) (Equation 8).

$$\eta_{power} = (\eta_{in-abs})(\eta_{in-trans}) + (\eta_{org-abs})(\eta_{org-diss})(\eta_{org-trans}) \quad (8)$$

the tunneling rates. Electric fields of this magnitude are not typically present in PV cells [37,41,43,48].

For SiNW/P3HT PV cell, the photon absorption in the SiNWs would be affected by the nanowires' morphology, band gaps, and the number of incident photons reaching them through the P3HT coating. The transportation of charge carriers in the SiNWs would be affected by their crystallinity, purity, morphology, and the band offset at the p-n junction [50].

With a band gap of 1.11 eV, Si can absorb over the entire visible spectrum, yet, since the optical absorption coefficient of Si decreases with crystallite size, the SiNWs would likely produce only one charge carrier pair per absorbed photon [51]. The band gaps of SiNWs are also dependent on the diameter as well as the orientation of the nanowires [27,52,53]. Under a diameter of approximately 2 nm, the band gaps of SiNWs may increase as much as 0.9 eV from that of bulk Si [51], and this affect is more pronounce in nanowires oriented in the [111] direction than the [110] direction [53]. Although deliberately increasing the band gaps of the SiNWs may not appear productive for photon harvesting, a bandgap of ~ 1.4 eV would still be sufficient to capture the entire visible spectrum [32] while providing some flexibility in tuning the band offset at the p-n junction. Figure 10 shows how the SiNW/P3HT PV cell could fail due to the disparity between the E_{OG} s of the two materials if the band offset is not properly aligned.

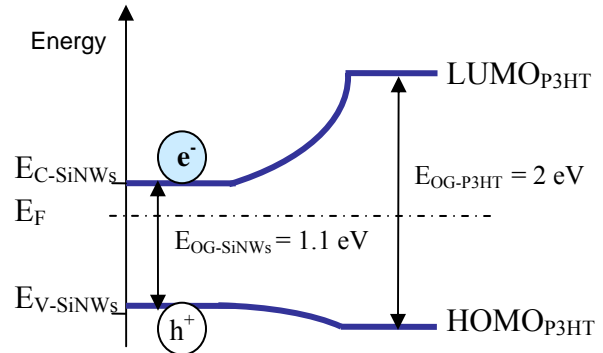


Figure 10: The disparity in the E_{OG} s between the SiNWs and the P3HT could result in a band offset which would not promote the transfer of charge carriers between the two semiconductors without an external bias.

Since the E_{OG} of the P3HT is around 2.0 eV [1,19], it would be possible for the E_V of the SiNW to be above the HOMO state of the P3HT, making the transfer of charge carriers between the two semiconductors energetically unfavorable without an external applied bias; charge carriers would build up on either side of the junction resulting in massive recombination losses. Indeed, due to the potentially

high level of crystallinity in SiNWs [54], the life spans and mobilities of the photogenerated charge carriers would be high, resulting in large recombination losses unless the internal electric potentials of the cell are sufficiently strong.

The use of SiNWs has additional advantages to bulk Si in that SiNWs have the potential for coherent and quantum transport of charge carriers, defects in one nanowire cannot directly affect the photo or electric properties of its neighbors, and the ability to modify the diameter, length and density of the nanowires allows control over the architecture of the p-n junction. Although the electron affinity of Si also scales with crystallite size [51], since the SiNWs would be anchored to a conducting substrate directly adjacent to the anode, the cell would not rely on percolation charge carrier transport, and this aspect of SiNWs would not be crucial to the functioning of the PV cell.

The PCE of the P3HT involves the photon absorption ($\eta_{org-abs}$), exciton dissociation ($\eta_{org-diss}$), and the transport of the charge carriers to the electrodes of the cell ($\eta_{org-trans}$) (Equation 8).

The factors influencing the photon absorption would be the E_{OG} , morphology, and the thickness of the P3HT layer. The E_{OG} s of the P3AT thin films are heavily dependent on morphology, but are typically around 2.0 eV [18,19,28,30,32,33]⁶. This is a bit narrow compared to the optical spectrum and can lead to a low I_{SC} [18,19,39,51] unless compensated for by either increasing the thickness of the film, incorporating lower E_{OG} materials, or introducing light trapping geometries [19]. In the context of the SiNW/P3HT PV cell, however, the SiNWs would be the optimal absorbers, and attempting to increase the photon harvest of the P3HT would be non-productive. The optical absorption coefficients of organic semiconductors can be relatively high⁷, and in order to optimize the percentage of photons passing through the P3HT film to become incident on the SiNWs, the P3HT layer should be no more than 100 nm thick [17,36].

Some photons would be absorbed into the P3HT layer, and the factors affecting the exciton transport and dissociation would be the degree of crystallinity, purity, and morphology of the film, the extent of the depletion region [42], and the band offset at the p-n

junction. Although it would be possible for excitons to dissociate at the depletion region formed at the junction between the P3HT and cell's cathode, this would not, in general, be productive towards photogenerated current due to recombination losses resulting from poor minority carrier mobility back through the polymer to the p-n junction [42].

The diffusion lengths of P3HT vary from 1-10 nm [8,17,29,36], and since excitons may diffuse in any direction during their lifetime, there exists an optimal distance of approximately 20 nm between depletion regions such that the exciton may reach a p-n junction before decaying or becoming trapped. The extent of the depletion region would be controlled by the doping concentration of the SiNWs, and the mobility of the minority carriers on either side of the hybrid heterojunction [55]. Because inorganic semiconductors have significantly higher carrier mobilities than organic semiconductors, the size of the depletion region would be considerably smaller on the side of the P3HT than on the SiNW side. Ideally, the two semiconductors would have similar E_{OG} with a large energy band offset at the p-n junction to insure exciton dissociation and attain as high a I_{SC} as possible while maintaining a large V_{OC} [32,36,39].

Charge carrier mobility in the P3HT would be affected by the degree of crystallinity [18,19,36,41], the morphology, and the purity [27,41] of the film. Due to the improved stacking of the molecules [18,31,32], regioregular P3HT would be preferable [56,57] with reported mobilities between $\sim 10^{-4}$ to $0.1 \text{ cm}^2 \text{V}^{-1} \text{s}^{-1}$ [29,58]. The degree of crystallinity in P3HT thin films may be controlled with the processing conditions (e.g. type of solvent used, substrate [17], atmosphere [59,60], and annealing [15,61]. Collection of charges at the cathode has been shown to be improved by a rougher P3HT/metal surface morphology [15].

Trap densities must remain low to assure a high FF [19], yet organic semiconductors are notoriously susceptible to air and moisture [17,27,36,48]⁸. The FF factor may also be improved by balancing the mobilities of charge carriers on either side of the p-n junction so that a bottleneck does not form at the hybrid heterojunction which would result in recombination losses [36].

Experimental Details

The SiNW were grown by vapor-solid (VS) and vapor-liquid-solid (VLS) methods. For both methods, a quartz horizontal furnace with electronic flow meters was used. Both methods employed 10 %

⁶ The E_{OG} s of P3ATs appear only slightly dependent on the chain length (i.e. varying by only ~ 0.2 eV between P3HT, P3OT, and P3DDT); in general, the longer the side chain, the larger the E_{OG} and the lower the optical absorption coefficient [18].

⁷ The optical absorption coefficients of the semiconducting polymers used in organic PV cell are on the order of 10^7 cm^{-1} [17,36].

⁸ There have been reports of P3HT prepared without protection from ambient conditions [18].

Si₂H₆ in Ar and 100 ppm PH₃ in Ar at a ratio of P:Si on the order of 10⁻³, with a total reactor pressure of 2 Torr.

For the VS method, a glass substrate coated with a 200 nm thin film of indium tin oxide (ITO) was used to nucleate the nanowires on small crystallite sites. The SiNWs were grown on the ITO surface at 410 °C for 10-15 min.

The VLS method utilized a Au:Si eutectic. The nanowires were grown for 10-15 min at 440 °C on a substrate of a-Si which had been dip coated in 3-mercaptopropyl-trimethoxysilane (MPTMS) before being dipped in Au nanoparticles suspended in de-ionized water. All the SiNWs were treated with HF to remove some of the SiO₂ prior to the application of the P3HT.

Due to the sensitivity of the P3HT to air and moisture, all procedures involving the P3HT were performed in a glove box under flowing N₂. The P3HT was purchased from Sigma Inc. as a semicrystalline powder and dissolved in xylene that had been bubbled with N₂ to remove oxygen. The P3HT was evaporated over the SiNWs at room temperature, however, a continuous thin film was not achieved. P3HT was also dropped onto a SiNW substrate and sandwiched with a top plate of ITO on glass; this also did not produce a continuous thin film.

Results and Discussion

The appearance of the SiNWs grown by VS method had a fuzzy camel color, whereas the SiNWs grown by the VSL method appeared fuzzy white. Although the low temperature processing should have helped prevent the diffusion of impurities, some from the Au from the eutectic apparently became incorporated into the bulk of the SiNWs, affecting their optical properties. Figure 11 shows a transmission electro microscopy (TEM) image of the VLS SiNWs. The nanowires grew in the [110] direction with no visible defects in the crystal lattice. They were 10-50 nm in diameter (depending on the size of the Au nanoparticles used) with an ~2 nm layer of SiO₂ covering the nanowires.

Figure 12 shows a scanning electron microscopy (SEM) image of the VLS SiNWs. The nanowires had grown into a mat several micrometers thick, with the density decreasing towards the top of the mat. The nanowires were 10-15 µm in length.

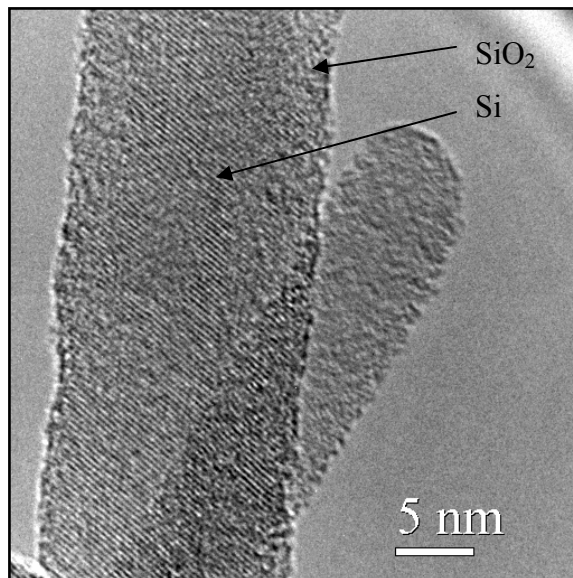


Figure 11: A TEM image of the SiNW showing a well ordered crystalline lattice with a SiO₂ coating ~2 nm thick.

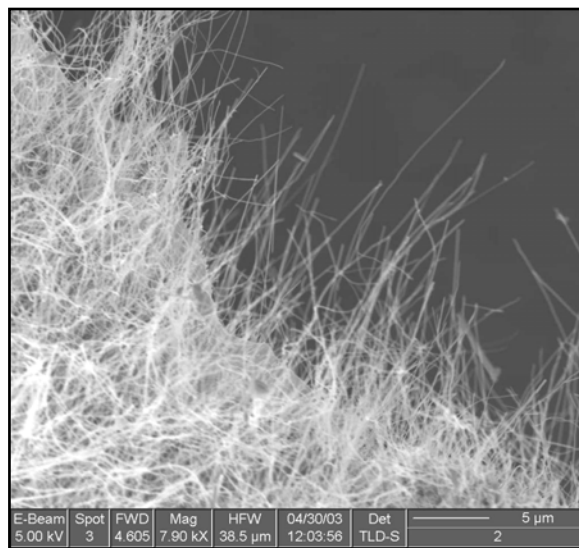


Figure 12: An SEM image of the SiNW grown on a-Si substrate using VLS method. The average distance between nanowires increases as the wires grow away from substrate.

Time of flight secondary ion-mass spectroscopy (TOFMS) gave the average P concentration for the bulk VLS SiNWs as $3.4 \times 10^{17} \text{ cm}^{-3}$. Energy dispersive X-ray spectroscopy (EDXS) of individual nanowires gave the P concentration at $3 \times 10^{18} \text{ cm}^{-3}$. Based on the estimated diffusion length of P in Si (assuming 450 °C for 30 min, this would be $\sim 2 \times 10^{-4} \text{ nm}$), diffusion was unlikely to be the doping mechanism for either type of SiNWs. Although the

thermodynamic mechanisms involved are not clear, the PH_3 apparently decomposed alongside the Si_2H_6 during the VS growth of the nanowires, likewise, the P in the VLS SiNWs became incorporated during formation despite the lack of a Au:P eutectic. EDXS from the VS SiNWs show no detectable levels of In or Sn from the ITO substrate.

The use of xylene for the dissolution of P3HT has been shown to produce higher efficiencies in polymer based PV cells than the use of chlorobenzene or chloroform [32,62]. However, the P3HT did not dissolve completely in the xylene, and since evaporation under a controlled atmosphere has produced well ordered thin films with low concentrations of impurities [10,63], this method is worth pursuing with other solvents. High quality thin films of P3HT may also be achieved with spin coating or screen printing, but these also require good solubility [19,42]. Other, less practical, options for the P3HT deposition, such as electropolymerization, which produces films of considerably lower order [48], or evaporation [19] which would require a lower molecular weight than what is readily commercially available and may not penetrate between the SiNWs, were disregarded.

Once a thin film of P3HT is achieved, preliminary investigations would include determining the optical absorption coefficient and carrier mobility of the film since both qualities are heavily dependent on morphology. Cyclic voltometry may be used to determine the oxidation/reduction potentials, and by utilizing a reference “half” electrochemical analysis [38] along with the optical absorption edge (which provides the E_{OG}), the absolute HOMO and LUMO levels may be estimated [18,38]. The Fermi level of the P3HT would be a fitted parameter of the completed cell as the degree of electrical shielding would be unknown [32].

The assembled SiNW/P3HT PV cell's I-V curve would give the I_{SC} , V_{OC} , and FF for the cell. UV-vis spectroscopy would be used to determine the absorption profile, electro-absorption for measuring the internal electric potentials, AC admittance to relate the performance of the cell to charge densities, and light induced electron-spin resonance to study the charge transport mechanisms [17]. Much of the optimizing parameters of the SiNW/P3HT PV cell would need to be empirically determined as the underlying physics of hybrid PV cells remains limited [32,41,64,65]⁹, as well as that of SiNW (e.g.

electro-optical effects of quantum confinement [50,51,53,54] and passivation [22,34]) and P3HT (e.g. the mechanism of excitation diffusion [34])

Choice of contacts also affects the function of the PV cell. Not only would a second depletion region be formed at the junction of both semiconductors with their respective contact, but any offset of the contacts' work function with the HOMO level of the P3HT and the E_{C} of the SiNWs would create additional electric potentials within the PV cell. Typically, a semiconductor adjacent to a metal forms a Schottky contact (i.e. voltage drops across the contact which would reduce the V_{OC} of the PV cell) [19,42], however, if the Fermi level of the electrode matches the E_{C} band of the inorganic semiconductor or the HOMO level of the organic semiconductor, an Ohmic contact may be established [31,66].

Some Au from the cathode of the SiNW/P3HT PV cell (as well as from the Au:Si eutectic in the VLS SiNWs) could diffuse into the P3HT over time, causing deep traps which, while they may facilitate charge generation and diffusion by providing “hopping” orbitals [38], would reduce the R_{SH} of the cell and thereby reduce the V_{OC} . Also, at any organic/metal contact, interfacial dipoles can significantly change the apparent work function of the metal [67,68], which would directly affect the V_{OC} of the PV cell [69]. Whether this would improve the energy level match at the organic/metal interface would need to be empirically determined, however it does introduce the option of additional coatings of another p-type polymer could be used to tune the Au cathode's work function [19]. Another option for the cathode would be ITO, which also possesses a work function susceptible to tuning via coating with high work function p-type polymers, such as PDOT [36], or by plasma etching [70]. Because ITO is transparent, it would be possible to create a top contact over the entire surface of the P3HT and thereby increase the I_{SC} of the cell. Polyethyldioxythiophene (PDOT) and polystyrenesulfonic acid (PSS) doped PDOT, which have higher work functions than ITO [18,19,42], have been utilized as cathodes in organic PV cells [71] and presents additional options for optimizing the V_{OC} of the SiNW/P3HT PV cell. Of course, the functionality of these polymers are also sensitive to morphology, solvents, and annealing [72]. A thin film of Al would be a prudent choice for the prototype SiNW/P3HT PV cell. Like Au, the Al work function may be tuned, but other low work function metals (e.g. Mg and Ca [39]) or polymers (e.g. PSS doped polyaniline (PANI)) [71] also exist.

Eventually, it would be desirable to replace the c-Si or ITO on glass as a SiNW substrates with a

⁹ Often, either the inorganic semiconductor is treated as a polymer with HOMO and LUMO levels and with loosely bound/widely dispersed excitons (Frenkel-Werner-Mott model [36,49]) or the organic semiconductor is approximated using the band model [10,26,27].

more economical polymeric substrate which would reduce the weight while providing some mechanical flexibility and durability to the PV cell. An organic polymer substrate would, however, introduce the potential of an oxide species forming on the Al contact which would also alter the metal's work function and the V_{OC} of the cell [18,19]. ITO may be coated on flexible foils of poly(ethyleneterephthalate) (PET) at ambient conditions [73] and there are several commercially available transparent flexible substrates: polyimide (Dupont Kapton), Tefzel, and Teflon [18]. The surface resistances and texture (i.e. PET, Kapton, and Tefzel are not flat) may require additional adhesive promoters [42].

One of the prominent advantages of the SiNW/P3HT PV cell's design would be the ability to utilize the pre-existing wet processing techniques and high throughput manufacturing of polymer industries [17,19]. However, considerations of the SiNW/P3HT PV cell's amortization should not be limited to production costs. Since the V_{OC} of organic PV cells have shown sensitivity to environmental contamination, light intensity [74,75], and temperature [74-76], the use of P3HT introduces these concerns into the proposed hybrid PV cell. The P3HT would require permanent protection from air and moisture, and its sensitivity to annealing introduces concerns about the ambient operating temperature of the cell continuing to chemically alter the polymer over time. Aid in addressing these disadvantages may be found in crossover research and development in the photodetector markets, as well as the organic FET and LED technologies [36,38].

Conclusion

Research into hybrid PV cells may provide the long sought after success of solar energy to supplant fossil fuels as a sustainable and ubiquitous energy source. Although much of the device physics involved in hybrid PV cells are not well understood, the functioning of PV cells may be easily modeled, and the optimizing parameters addressed experimentally. The materials of the proposed SiNW/P3HT PV cell are high performance and possess tunable properties well suited for experimental optimization. SiNWs and P3HT are also the subjects of intensive study in multiple technologies, providing crossover research and development for the progress of the SiNW/P3HT PV cell.

Although a completed SiNW/P3HT PV cell has not yet been achieved due to the inability to form a thin film of P3HT, research into this design will continue.

Acknowledgements

This research was funded by the McNair Program at Portland State University. Special thanks to Keith James, Katherine Mazzio, and Kaitlyn VanSant for their many helpful comments.

References

1. US Department of Energy Report, Basic needs for solar energy utilization, Chair: N. S. Lewis, (2005) http://www.sc.doe.gov/bes/reports/files/SUE_rpt.pdf
2. International Energy Agency-Photovoltaic Power Systems Programme Report, Trends in Photovoltaic Applications, Chair: S. Nowak, (2004) http://www.iea-pvps.org/products/download/rep1_13.pdf
3. M. D. McGehee, et al., GCEP Technical Report (2005), <http://gcep.stanford.edu>
4. K. R. Catchpole, et al., (2000), [dSPACE.anu.edu.au, http://hdl.handle.net/1885/40863](http://hdl.handle.net/1885/40863)
5. Y. S. Tsuo, et al., NREL/CP-590-23902 (1998) <http://www.nrel.gov/ncpv/pdfs/tsuo.pdf>
6. M. D. Archer, et al., Clean Electricity From Photovoltaics, Imperial College Press, London (2001)
7. A. Breeze, et al., NREL/CP-590-33580 (2003), <http://www.nrel.gov/docs/fv03osti/33580.pdf>
8. W. U. Huynh, et al., Science **295**, 29 (2005)
9. A. Du Pasquier, et al., App. Phys. Lett. **87**, 203511 (2005)
10. C. Y. Kwong, Chem. Phys. Lett. **384**, 372-375 (2004)
11. N. S. Sariciftci, Mat. Today **36-38** (2004)
12. G. Li, et al., SPIE Newsroom, 10.1117/2.1200603.0147 (2006), <http://newsroom.spie.org/x2976.xml?highlight=x517>
13. L. M. Campos, et al., Chem. of Mat. **17**, 16 (2005), <http://www.ipc.uni-linz.ac.at/publ/2005/2005-028.pdf>
14. J. Nuzi, C. R. Physique **3**, 523-542 (2002)
15. G. Li, et al., J. of App. Phys **98**, 043704 (2005)
16. J. Rostalski, et al., Solar Energy Materials & Solar Cells **63**, 37-47 (2000)
17. J. Nelson, Current Opinion in Solid State and Materials Science **6**, 87-95 (2002)
18. M. Al-Ibrahim, et al., Organic Electronics **6**, 65-77 (2005)
19. H. Hoppe, et al., J. Mater. Res. **19**, 1924-1945 (2004)
20. (20(3)) L. Bozano, et al., App. Phys. Lett. **74**, 1132-1134 (1999)
21. K. M. Coakley, et al., Chem. Mater. **16**, 4533 (2004)
22. M. K. Nazeeruddin, et al., J. Am. Chem. Soc. **115**, 6382-6390 (1993)
23. M. Graetzel, Current Opinion in Colloid & Interface Science **4**, 314-321 (1999)
24. E. Arici, Encyclopedia of Nanoscience and Nanotechnology **3**, 929-944 (2004)
25. J. Lui, et al., J. Am. Chem. Soc. **126**, 6550-6551 (2004)
26. H. Baessler, Molecular Crystals and Liquid Crystals Science and Technology **252**, 11-21 (1994)
27. A. P. Alvisatos, NREL/SR-520-34567 (2003), http://www.osti.gov/energycitations/product.biblio.jsp?osti_id=15004565
28. I. Riedel, et al., Phys. Stat. Sol. **201**, 1332 (2004)

29. H. Sirringhaus, et al., Science **280**, 1741 (1998)
30. F. Padinger, et al., Adv. Funct. Mater. **13**, 85 (2003)
31. W. U. Huynh, et al., Phys. Rev. B **67**, 115326 (2003)
32. Y. Terada, et al., J. App. Phys. **97**, 124302 (2005)
33. G. Dicker, et al., Synth. Met. **137**, 863 (2003)
34. P. A. Thrower, Materials in Today's World, Second Edition, McGraw-Hill (1996)
35. S. N. Novikov, et al., Adv. Colloid Interface Sci. **105**, 329-39 (2003)
36. J. M. Kroon, et al., European Photovoltaic Solar Energy Conference and Exhibition, Barcelona, Spain (2005)
37. J. Simon, et al., Molecular Semiconductors, Springer-Verlag Berlin Heidelberg New York Tokyo, (1985)
38. S. Sun, et al., J. Mater. Sci. **40**, 1429-1443 (2005)
39. R.H. Friend, Pure App. Chem, **73**, 425-430 (2001)
40. Z. G. Soos, et al., *Correlations in Conjugated Polymers*, Conjugated Polymers: Molecular Exciton versus Semiconductor Band Model, Edited by N.S. Sariciftci, World Scientific, Singapore (1997) <http://www.ipc.unilinz.ac.at/publ/book/Chapter1.pdf>
41. B.A. Gregg, et al., J. Appl. Phys. **93**, 3605-3614 (2003)
42. V. K. Basavaraj, et al., IEE Proc. Circuits Devices Syst. **150**, 6 (2003)
43. R. Schroeder, Doctoral Thesis, Virginia Polytechnic Institute and State University, Virginia, USA (2001)
44. M. Kuno, et al., J. App. Phys. **106**, 9869 (1997)
45. J.J. Dittmer, et al., Adv. Mater. **12**, 1270, (2000)
46. Z. A. Peng, et al., J. Am. Chem. Soc. **123**, 1389 (2001)
47. C. J. Brabec, et al., Adv. Funct. Mater. **11**, 374 (2001)
48. G. Horowitz, Adv. Mater. **10**, 365-377 (1998)
49. V. M. Agranovich, et al., Pure Appl. Opt. **7**, 119-127 (1998)
50. R. Wang, et al., Phys. Rev B **61**, 16827-16832 (2000)
51. M. Nirmal, et al., Acc. Chem. Res. **32**, 407-414 (1999)
52. D. Katz, et al., Phys. Rev. Lett. **89**, 086801 (2002)
53. X. zhao, et al., Phys. Rev. Lett. **92**, 2368051 (2004)
54. B. Li, et al., Phys. Rev. B **59**, 1645-1648 (1999)
55. D. Meissner, et al., SPIE Proc. **1729**, Toulouse, 24-35 (1992)
56. T. A. Chen, et al., J. Am. Chem. Soc. **117**, 233 (1995)
57. N. Camaioni, et al., Synth. Met. **125**, 313 (2002)
58. A. Assadi, et al., Appl. Phys. Lett. **53**, 195 (1988)
59. A. C. Arias, et al., Macromolecules **34**, 6005-6013 (2001)
60. L. S. Roman, et al., Adv. Mat. **12**, 189 (2000)
61. N. Camaioni, et al., Adv. Mat. **14**, 1735 (2002)
62. R. Schroeder, PhD Thesis, Virginia Polytechnic Institute and State University (2001)
63. K. E. Strawhecker, et al., Macromolecules **34**, 4669 (2001)
64. Y. Chi, et al., J. Phys. Chem. B **104**, 5213 (2000)
65. D. S. Ginger, et al., Synth. Met. **124**, 117 (2001)
66. G. Yu, et al., Science **270**, 1789 (1995)
67. I. H. Campbell, et al., Phys. Rev. B **54**, 14321 (1996)
68. C. D. Dimitrakopoulos, et al., IBM J. Res. Dev. **45**, 11 (2001)
69. H. Frohne, et al., Chem. Phys. Chem. **9**, 795 (2002)
70. K. Sugiyama, et al., J. Appl. Phys. **87**, 295 (2000)
71. S. A. Cater, et. al., Appl. Phys. Lett. **70**, 2067-2069 (1997)
72. S. K. M. Joenssona, et al., Synth. Met. **139**, 1 (2003)
73. S. Sensfuss, et al., Synth. Met. **137**, 1433 (2003)
74. I. Riedel, et al., Adv. Funct. Mat. **14**, 38 (2004)
75. V. Dyakonov, et al., Sol. Energy Mat. Sol Cells **61**, 53 (2000)
76. E. A. Katz, et al., J Appl. Phys. **90**, 5343 (2001)